

Deblurring Neural Radiance Fields with Event-driven Bundle Adjustment

Yunshan Qi
Beihang University
qi_yunshan@buaa.edu.cn

Lin Zhu
Beijing Institute of Technology
linzhu@bit.edu.cn

Yifan Zhao
Beihang University
zhaoyf@buaa.edu.cn

Nan Bao
Beihang University
nbao@buaa.edu.cn

Jia Li
Beihang University
jiali@buaa.edu.cn

ABSTRACT

Neural Radiance Fields (NeRF) achieve impressive 3D representation learning and novel view synthesis results with high-quality multi-view images as input. However, motion blur in images often occurs in low-light and high-speed motion scenes, which significantly degrade the reconstruction quality of NeRF. Previous deblurring NeRF methods are struggling to estimate information during the exposure time, unable to accurately model the motion blur. In contrast, the bio-inspired event camera measuring intensity changes with high temporal resolution makes up this information deficiency. In this paper, we propose Event-driven Bundle Adjustment for Deblurring Neural Radiance Fields (EBAD-NeRF) to jointly optimize the learnable poses and NeRF parameters by leveraging the hybrid event-RGB data. An intensity-change-metric event loss and a photo-metric blur loss are introduced to strengthen the explicit modeling of camera motion blur. Experiment results on both synthetic data and real captured data demonstrate that EBAD-NeRF can obtain accurate camera poses during the exposure time and learn sharper 3D representations compared to prior works.

CCS CONCEPTS

- Computing methodologies → Shape representations.

KEYWORDS

Neural radiance fields, event camera, image deblurring, novel view synthesis

1 INTRODUCTION

Neural Radiance Fields (NeRF) [29] achieve 3D implicit representation learning and photo-realistic novel view synthesis results with high-quality 2D images and precise camera poses as input. In low-light scenes, a camera often requires a longer exposure time to obtain an image with sufficient brightness [54]. A hand-held camera or a moving camera may cause motion blur in the captured image. Moreover, a high-speed moving camera can also cause motion blur, even in bright scenes with short exposure time. The blurred images will cause NeRF to learn a blurry 3D implicit representation, resulting in degraded quality of the synthesized novel view image. Thus, reconstructing sharp NeRF from blurry images is a practical problem for 3D reconstruction in low-light scenes [51].

Motion blur is essentially caused by the camera pose change during exposure time. Recent deblurring NeRF works try to model the camera motion and optimize the estimated camera pose change

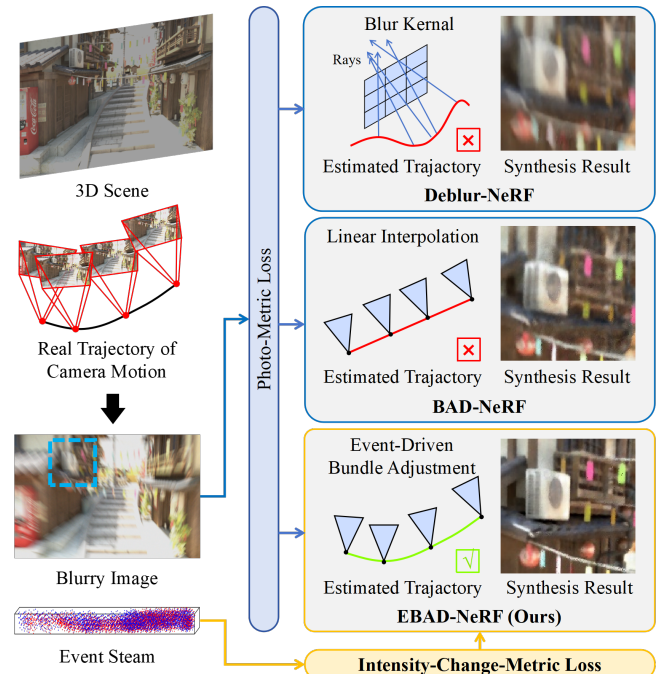


Figure 1: Motivation of our proposed method. In a low-light scene or with a high-speed moving camera, motion blur usually occurs in the captured images. To reconstruct sharp NeRF from blurry images, Deblur-NeRF [26] uses a deformable sparse kernel to model the blur process. BAD-NeRF [44] linearly interpolates the camera poses and jointly learns the start and end poses of camera motion. However, these methods are unable to model complex motion blur and lack supervision information during exposure time with only a photo-metric loss. With the proposed event-driven bundle adjustment, our EBAD-NeRF can recover the accurate camera motion trajectory and consequently reconstruct sharper novel view images with sharper learned NeRF.

with photo-metric loss [26, 33, 44]. As shown in Figure 1, Deblur-NeRF [26] propose the deformable sparse kernel (DSK) module to simulate the change of rays from the camera. The camera motion trajectory of blur is implicitly learned in an additional multilayer perceptron (MLP), which is unstable when facing complex and severe motion blur. BAD-NeRF [44] uses linear interpolation to

model the motion trajectory. The starting and ending poses of the trajectory are jointly optimized with the parameters of NeRF. This strategy works well for most motion blur, but a handheld camera is not necessarily shaking linearly under long exposures, and this could lead to a failure of reconstruction under the linear interpolation modeling. Although the previous works have tried different motion blur modeling methods for deblurring NeRF, relying solely on photo-metric loss cannot form effective constraints on the camera trajectory estimate. Because there is inherent information loss within the exposure time in the input blurred image, and the modeling is limited by this. The bio-inspired event camera can measure brightness changing asynchronously with high temporal resolution [8], which can make up for the information loss of blurry images. Recently, E²NeRF [33] uses both event data and blurry images to model the blur in terms of image formation and achieved better results than the image-based deblurring works. However, camera poses of this work are obtained by pre-deblurred images and are not learnable, which limits its performance.

In this paper, we use learnable poses to model the camera motion trajectory. Event data is introduced into the camera pose learning by conducting an additional intensity-change-metric loss to effectively optimize the changes in adjacent poses. Unlike previous image-based works with only blurry images as supervision, which lacks constraints within the camera pose changes, we are able to fit the camera poses to the real motion trajectory during the blurring process and achieve sharper NeRF reconstruction. Specifically, for each view, we first use multiple learnable camera poses to model the camera motion trajectory and transfer them into the SE(3) space [4, 44]. During the training, we jointly optimize these poses and the parameters of the NeRF network. A photo-metric blur loss is also used to supervise the modeling of blurry image formation. We introduce an intensity-change-metric event loss to supervise pose changes during the exposure time. The image formation is additionally strengthened by the event loss. The framework can estimate an accurate camera trajectory corresponding to the input blurry image, and a sharper NeRF is learned. We extend 5 blender synthetic scenes in Deblur-NeRF with event data and use a DAVIS-346 event camera [42] to capture spatial-temporal aligned Event-RGB (ERGB) data with ground truth. Experiments on both synthetic data and real data demonstrate that our method can learn sharper neural radiation fields and more accurate camera motion trajectories compared with image deblurring methods and deblurring NeRF methods. To summarize, we present the following contributions:

- 1) A novel event-driven bundle adjustment deblurring neural radiance fields (EBAD-NeRF) framework is proposed to explicitly model image blur and jointly optimize the estimated camera motion trajectory and NeRF parameters.
- 2) An intensity-change-metric event loss and a photo-metric loss are presented to supervise the modeled motion blur in terms of both camera pose change and image formation conjugatively.
- 3) Experiments on both extended synthetic data and real captured data validate that our method achieves accurate motion trajectory estimation and high-quality 3D implicit reconstruction of the scene with severe blurry images and corresponding event data.

Table 1: Comparison of Previous Deblurring NeRF Works

Method	RGB Event	Motion Blur Model
Deblur-NeRF	✓	-
DP-NeRF	✓	-
Sharp-NeRF	✓	-
BAD-NeRF	✓	-
E ² NeRF	✓	✓
EBAD-NeRF	✓	✓
		Event-driven
		Bundle Adjustment

2 RELATED WORK

2.1 Neural Radiance Fields

The neural radiation fields model achieves impressive novel view synthesis results and inspires a lot of subsequent research [9]. For example, [2, 3, 43, 50] improve the quality of learned geometry and synthesized novel views. Other works try to improve the training and rendering speed such as FastNeRF [10], MobileNeRF [7] and EfficientNeRF [15]. PixelNeRF [52] and RegNeRF [30] realize reconstructing high-quality NeRF with few input views. RawNeRF [28] can recover a clean NeRF from noisy raw images. HDR-NeRF generates high dynamic novel view images with low dynamic images as input. Besides, nerf also requires accurate camera poses from COLMAP as input. BARF [23], L2G-NeRF, and Nope-NeRF [5] explore reconstructing NeRF when camera poses are not provided.

Blurry Images are often captured in low-light scenes or with a high-speed moving camera on drones or robots. Reconstructing sharp NeRF from blurry images also becomes a challenging problem. As shown in Table 1, Deblur-NeRF [26] proposes a deformable sparse kernel module to effectively model the blurring process. However, the blurring kernel is optimized based on 2D-pixel location independently. DP-NeRF [22] proposes a rigid blurring kernel and generates a 3D deformation field, which is constructed as the 3D rigid motion of the camera for each view. Sharp NeRF [21] proposed a learnable grid-based kernel to obtain sharp output from neural radiance fields. Inspired by BARF, BAD-NeRF [44] conducts linear interpolation for the camera poses during the exposure time and jointly optimizes the poses with bundle adjustment.

2.2 Image Deblurring

Traditional deblurring algorithms focus on finding the suitable blur kernel of a blurry image to recover a sharp image. Hand-crafted features or sparse priors are used to tackle this problem blur [6, 20, 49]. Deep learning deblurring works directly learn an end-to-end mapping from blurry to sharp images [40, 45, 59]. MPRNet [53] and SRN [41] achieve impressive single-image deblurring results. In addition to single-image deblurring, [19, 55, 56] proposes deblurring schemes for continuous video images, which used the characteristics of video images(such as temporal consistency) to better predict sharp images, but this also brought greater calculation amount. He *et al.* [14] weights a combination of input images to avoid explicit calculation of blur kernels and effectively improves processing speed. Other works have also tried implementing multiple image deblurring using convolutional neural network and Unet framework

[38, 46]. Son *et al.*[37] proposes an effective recurrent video deblurring network and achieves state-of-the-art performance. However, the information missing from blurry images during exposure time makes the robustness of the image-based method decreases in the face of various motion blur.

2.3 Event Camera

Event camera is based on a bio-inspired vision sensor that measures brightness changing asynchronously [8]. The high temporal resolution and high dynamic visual data capturing paradigm makes event cameras ideal for flow estimation [1, 11, 13, 31, 36], feature detection and tracking[48, 57, 58] and images deblurring [24, 32, 35, 47]. Pan *et al.* [32] propose a simple event-based double integral model (EDI) based on event generation to establish the connection between blurry images and events. Shang *et al.* [35], Jiang *et al.*[18] and Sun *et al.* [39] using learning-based network to recover sharp images with events.

Recently, event-based NeRF works have emerged. Ev-NeRF [17] models the measurement of the event sensor to learn grayscale neural radiance fields derived from the event stream. EventNeRF [34] reconstructs color NeRF with a color event camera. *e*-NeRF [25] improves Ev-NeRF and EventNeRF for non-uniform camera motion. DE-NeRF [27] uses both RGB images and events to learn a deformable NeRF. E²NeRF first reconstructs a sharp NeRF with blurry images and corresponding event data and achieves state-of-the-art performance. However, it only explicitly models the blurring processing at the imaging aspect. For camera motion during the exposure time, E²NeRF relies on pre-deblurred images with EDI [32] algorithm and structure-from-motion method COLMAP for pose estimation. Notably, our proposed EBAD-NeRF transforms camera motion trajectories into a learnable model with event-driven bundle adjustment. The framework unlocks the potential of event information in explicit modeling of blur processing at the level of both image changes and camera motion.

3 METHOD

We introduce EBAD-NeRF to simultaneously learn the poses of the camera’s motion process and generate sharp neural radiance fields using both blurred images and the event stream within the corresponding exposure time. Events serve two key purposes within the framework: (1) optimizing camera trajectories within the exposure time, and (2) contributing to the physical formation of motion blur in the image by providing information on light intensity changes. Moreover, we employ a photo-metric blur loss to supervise blur formation in the RGB domain. Figure 2 shows the overview of our approach. Sec. 3.1 introduces the motion blur formation in the neural radiance fields. Sec. 3.2 illustrate the proposed event-driven bundle adjustment method. Sec. 3.3 shows the loss function and the derivation, and Sec. 3.4 describes the implementation details of our method.

3.1 Motion Blur Formation in Static 3D Scene

In a static 3D scene, camera motion blur is caused by the changes of camera pose \mathbf{P} during the exposure time. A digital image \mathcal{I} is obtained by measuring the integration of light intensity I on the

image sensor.

$$\mathcal{I} = \int_{t_{start}}^{t_{end}} I(t) dt, \quad (1)$$

where t_{start} and t_{end} is the start and end time of exposure. The light intensity I is only corresponding to the camera pose, and we can express \mathbf{P} as a function of time $\mathbf{P} = p(t)$. Then, a blurry image \mathcal{B} can be expressed as:

$$\mathcal{B} = \int_{t_{start}}^{t_{end}} I(p(t)) dt. \quad (2)$$

In NeRF [29], the rendering results are closely related to camera poses. Given a camera pose $\mathbf{P} = p(t)$, for each pixel of the imaging plane, we can obtain a ray \mathbf{r} that emits from the optical center of the camera and passes through the pixel \mathbf{x} . With stratified sampling, we can divide the part of this ray starting with l_{near} and ending with l_{far} into N equal parts and randomly sample points in each part. For each of the N sampled points, we input the 3D coordination \mathbf{o} in the world coordinate system and 2D view the direction \mathbf{d} represented by the ray \mathbf{r} into NeRF MLP F_θ with network parameters θ :

$$(\mathbf{c}, \sigma) = F_\theta(\gamma_o(\mathbf{o}), \gamma_d(\mathbf{d})), \quad (3)$$

the output of which is color \mathbf{c} and density σ and $\gamma(\cdot)$ is an encoder for a higher $K + 1$ dimension of input of the network:

$$\gamma_K(x) = \{\sin(2^k \pi x), \cos(2^k \pi x)\}_{k=0}^K. \quad (4)$$

Then, we can obtain N colors $\{\mathbf{c}_i\}_{i=1}^N$ and densities $\{\sigma_i\}_{i=1}^N$ of the sampled points. By conducting volume rendering:

$$C(\mathbf{r}, \mathbf{x}) = \sum_{i=1}^N T_i (1 - \exp(-\sigma_i \delta_i)) \mathbf{c}_i, \quad (5)$$

where $T(i) = \exp(-\sum_{j=1}^{i-1} \sigma_j \delta_j),$

we can get the final color value of the pixel \mathbf{x} passed by the ray \mathbf{r} corresponding to the pose \mathbf{P} . $\delta_i = l_{i+1} - l_i$ is the distance between adjacent sampled points, and T_i is the transparency between l_n and sampled point.

If we assume that the learned NeRF MLP is sharp, we can model the image motion blur by discretizing Eq. (2) with p poses $\{\mathbf{P}_i\}_{i=1}^p$ sampled evenly over the exposure time:

$$\hat{\mathcal{B}}(\mathbf{x}) = \frac{1}{p} \sum_{i=1}^p C(P(t), \mathbf{x}), \mathbf{x} \in \mathcal{X}, \quad (6)$$

where \mathcal{X} represents the pixels of the image sensor. Since we use virtual sharp image color $C(P(t), \mathbf{x})$ to replace the light intensity $I(P(t))$, we need to multiply each item by a weight of time in Eq. (6). As the poses are temporally evenly sampled, we can directly use an average $\frac{1}{p}$ to represent the weight.

At this point, we have established the connection between image motion blur, camera pose, and neural radiation field.

3.2 Event-driven Bundle Adjustment

In BAD-NeRF [44], only the start pose \mathbf{p}_1 and end pose \mathbf{p}_p of the exposure time is parameterized and learned, and the motion process is represented with a linear model. This approach may fail in long exposure or high-speed situations where the camera is likely to

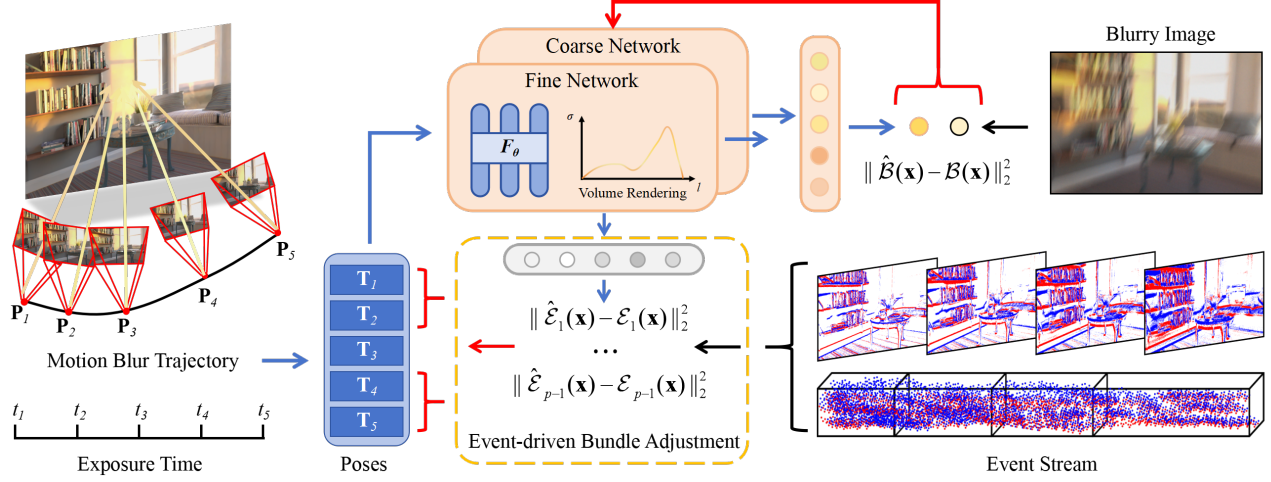


Figure 2: Overview of our method. An image with motion blur is caused by the camera moving during the exposure time. We temporal evenly sample p poses $\{P_i\}_{i=1}^p$ and transfer them into $SE(3)$ as learnable parameters. Then, the poses are input into the NeRF network to model the blurry image and event stream generation. The intensity-change-metric loss can optimize the modeling in terms of camera motion. The photo-metric loss can optimize and optimize the modeling in terms of image formation. With the joint learning of NeRF parameters θ and camera poses, a sharp NeRF is learned eventually.

have complex motion (non-uniform motion, curved motion) during exposure time. In order to better fit the camera motion trajectory, we express the camera poses $\{P_i\}_{i=1}^p$ as $\{T_i\}_{i=1}^p \in SE(3)$.

At this time, in addition to recovering the starting and ending poses, the motion trajectory modeling must also find the relationship between adjacent poses. We can model this correlation by modeling the generation of events, which measures the light intensity change in the log domain asynchronously:

$$E(t_1, t_2) = \begin{cases} \lfloor \frac{\log(I(t_2)) - \log(I(t_1))}{\Theta} \rfloor, & I(t_2) \leq I(t_1) \\ \lceil \frac{\log(I(t_2)) - \log(I(t_1))}{\Theta} \rceil, & I(t_2) > I(t_1) \end{cases}. \quad (7)$$

Note that we round the modeled events because an event is only triggered when the light intensity change threshold reaches Θ .

According to previous event simulation work, V2E [16], we can convert the color of the images into grayscale and model the event generation. Based on this, the estimated event data can be expressed by bringing the predicted color in Eq. (5) into Eq. (7):

$$\hat{E}(t_1, t_2) = \begin{cases} \lfloor \frac{\log(\bar{C}(T(t_2))) - \log(\bar{C}(T(t_1)))}{\Theta} \rfloor, & \bar{C}(t_2) \leq \bar{C}(t_1) \\ \lceil \frac{\log(\bar{C}(T(t_2))) - \log(\bar{C}(T(t_1)))}{\Theta} \rceil, & \bar{C}(t_2) > \bar{C}(t_1) \end{cases}, \quad (8)$$

where $\bar{C}(\cdot)$ means taking the average on the RGB channels to get the intensity value.

The computation of $\hat{E}(x, t_1, t_2)$ is differentiable with respect to $\{T_i\}_{i=1}^p$, and we can jointly optimize the sampled camera poses and parameters of F_θ by using actual events as supervision.

3.3 Loss Functions

We introduce the intensity-change-metric event loss to optimize the camera motion poses $\{T_i\}_{i=1}^p$ during exposure time as well as the NeRF parameter θ by minimizing the differences between the numbers of predicted and actual events on all pixels $x \in \mathcal{X}$:

$$\mathcal{L}_{event} = \frac{1}{p} \sum_{k=1}^{p-1} \|(\hat{E}_k(t_k, t_{k+1})) - (E_k(t_k, t_{k+1}))\|_2^2. \quad (9)$$

In the training phase, we only calculate the event loss between adjacent sampling poses because if the sampling frames are far apart, the event loss will fluctuate greatly, thus affecting the stability of the network.

We also conduct the photo-metric blur loss between the predicted and the input blurry images:

$$\mathcal{L}_{blur} = \|\hat{B}(x) - B(x)\|_2^2, \quad (10)$$

which also has a constraint on both the camera poses and neural radiance fields, as proved in BAD-NeRF. To strengthen the learning, the final loss is the sum of \mathcal{L}_{event} and \mathcal{L}_{blur} :

$$\mathcal{L}_{blur} = \lambda \mathcal{L}_{event}^c + \mathcal{L}_{blur}^c + \mathcal{L}_{blur}^f, \quad (11)$$

where λ is a weight parameter of event loss. We used the design of the fine and coarse network in NeRF to conduct blur loss \mathcal{L}_{blur}^f and \mathcal{L}_{blur}^c on both of the networks. Event loss \mathcal{L}_{event}^f is only calculated for the fine network because it can render enough texture details for event estimation.

The learnable camera poses $\{T_i\}_{i=1}^p$ and NeRF parameter θ are optimized by the Jacobians of event loss:

$$\frac{\partial \mathcal{L}_{event}}{\partial \theta} = \frac{\partial \mathcal{L}_{event}}{\partial \mathcal{E}(x)} \cdot \frac{1}{m} \sum_{x \in \mathcal{X}} \frac{\partial \mathcal{E}(x)}{\partial C(x)} \frac{\partial C(x)}{\partial \theta}, \quad (12)$$

$$\frac{\partial \mathcal{L}_{event}}{\partial \mathbf{T}_i} = \frac{\partial \mathcal{L}_{event}}{\partial \mathcal{E}(\mathbf{x})} \cdot \frac{1}{m} \sum_{\mathbf{x} \in \mathcal{X}} \frac{\partial \mathcal{E}(\mathbf{x})}{\partial C(\mathbf{x})} \frac{\partial C(\mathbf{x})}{\partial \mathbf{T}_i}, \quad (13)$$

and the Jacobians of blur loss:

$$\frac{\partial \mathcal{L}_{blur}}{\partial \theta} = \frac{\partial \mathcal{L}_{event}}{\partial \mathcal{B}(\mathbf{x})} \cdot \frac{1}{m} \sum_{\mathbf{x} \in \mathcal{X}} \frac{\partial \mathcal{B}(\mathbf{x})}{\partial C(\mathbf{x})} \frac{\partial C(\mathbf{x})}{\partial \theta}, \quad (14)$$

$$\frac{\partial \mathcal{L}_{blur}}{\partial \mathbf{T}_i} = \frac{\partial \mathcal{L}_{blur}}{\partial \mathcal{B}(\mathbf{x})} \cdot \frac{1}{m} \sum_{\mathbf{x} \in \mathcal{X}} \frac{\partial \mathcal{B}(\mathbf{x})}{\partial C(\mathbf{x})} \frac{\partial C(\mathbf{x})}{\partial \mathbf{T}_i}, \quad (15)$$

where m is the number of pixels of the image.

Then, the network can learn an accurate camera motion and sharp 3D implicit representation with gradient propagation.

3.4 Implementation Details

We train the EBAD-NeRF on a single NVIDIA RTX 3090 GPU. The training time has not increased compared with BAD-NeRF because there is no extra rendering computation for event loss. The sample number of the rays $N = 64$ for fine and coarse networks. The number of sampled poses of each view p is set to 4, and the weight of event loss λ is set to 0.005. Sec.4.4 evaluates the influence of the parameters. Additionally, we use $\Theta = 0.3$ as the threshold of the event generation, which is a typical value in event-based vision [8]. A coarse initial pose for each view is given at the start of training.

4 EXPERIEMENTS

4.1 Datasets

4.1.1 Synthetic Data: We extend five Blender scenarios of Deblur-NeRF (Cozyroom, Factory, Pool, Tanabata, and Wine). (1) We increase the camera shake amplitude of the Factory, Pool, Tanabata, and Wine scenes to increase the blur degree of the training images and maintain the camera shaking in Deblur-NeRF of the Cozyroom scene to evaluate the effect of different shaking scales. (2) During the camera motion, we added the speed changes often occurring when the hand-held camera shakes. (3) To generate corresponding event data, we input the virtual sharp frames of the camera shake process rendered by Blender into the event simulation tool V2E [16] to generate the corresponding event stream.

4.1.2 Real Data: To test the effectiveness of our method on real captured data, we captured two sets of real data using the DAVIS-346 [42] event camera, which can capture spatial-temporal aligned event data and RGB data at the same time. Both sets of data are captured in low-light scenes, so a longer exposure time (100ms) is needed for RGB data to get a bright enough image. We use a handheld camera to capture training data with blur and a tripod to mount the camera to capture sharp testing data. Each scene contains 16 views of blurry images and corresponding events for training and 4 novel view sharp images for training.

4.2 Comparing Method

4.2.1 Image Deblurring Method: For comparison, we selected two classic learning-based image deblurring methods, MPR [53] and SRN [41]. In order to make a more fair comparison in terms of data modalities, we selected the D2Net method, which also uses event and image modal data fusion to achieve image deblurring. We input the images deblurred by these three methods into the

Table 2: Quantitative Ablation Study on the Tanabata Scene.

	PSNR↑	SSIM↑	LPIPS↓	ATE
BAD-NeRF	20.65	.7567	.3349	0.0514 ± 0.0204
EBAD-NeRF-noe	22.00	.7961	.3728	0.0462 ± 0.0183
EBAD-NeRF-linear	23.75	.8478	.2881	0.0418 ± 0.0160
EBAD-NeRF-full	24.99	.8800	.2069	0.0301 ± 0.0122

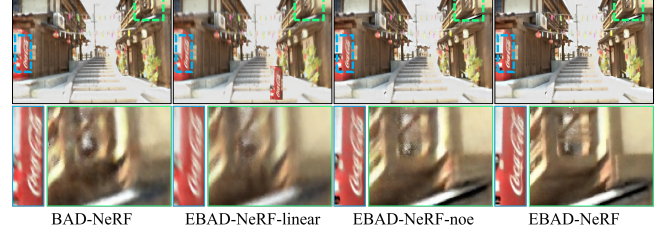


Figure 3: Qualitative Ablation Study on the Tanabata Scene. EBAD-NeRF-linear and EBAD-NeRF-noe are defined in Sec. 4.3. With event-driven bundle adjustment, the rendering results of learned NeRF are sharper and clearer.

original NeRF for the novel view generation task to learn a sharp 3D representation.

4.2.2 Deblurring NeRF Method: We selected image-based deblurring NeRF method Deblur-NeRF [26] and BAD-NeRF [44] and ERGB-dual-modal-based deblurring NeRF method E²NeRF [33] for comparison. For Deblur-NeRF, we use the default parameters for the spare deformation kernel. For BAD-NeRF, we use the number of interpolated virtual cameras as 7 to get sufficiently satisfactory results, as described in the paper. For E²NeRF, we follow the paper and use $b = 4$ to train the model. All NeRF-based methods are trained with 5000 rays of batch size and 64 sampling points for coarse and fine networks. We perform 100,000 iterations on synthetic data. On real data, due to the reduction in image resolution and the number of views, 50,000 iterations are enough for all NeRF-based methods to converge to good enough results.

4.2.3 Metrics: We use PSNR, SSIM, and LPIPS [60] to evaluate the NeRF reconstruction results and use absolute trajectory error (ATE) to evaluate the fitting accuracy of the camera motion trajectory [12].

4.3 Event-driven Bundle Adjustment Analysis

We analyze the proposed event-driven bundle adjustment at two levels: 3D reconstruction quality and motion trajectory fitting accuracy. As shown in Table 2, Figure 3 and Figure 4, EBAD-NeRF-noe training proposed EBAD-NeRF without event data as supervision. EBAD-NeRF-linear represents the results of adding event data constraints to BAD-NeRF directly.

4.3.1 Defect of Linear Interpolation Bundle Adjustment: The quantitative results in Table 2 demonstrate that without event enhancement, the bundle adjustment constrained by linear interpolation

Table 3: Quantitative Results on Deblurring Views of Blender Scenes. The Best Results are Shown in Bold.

	Cozyroom			Factory			Pool			Tanabata			Wine			Average		
	PSNR↑	SSIM↑	LPIPS↓															
NeRF	27.04	.9034	.2875	20.54	.6776	.5233	27.39	.8352	.4356	19.13	.6691	.5743	20.11	.6732	.5832	22.84	.7517	.4808
D2Net	28.25	.9271	.2083	21.15	.7096	.4428	28.23	.8589	.3537	19.34	.6947	.4973	20.60	.6977	.4894	23.52	.7776	.3983
NeRF+D2Net	28.11	.9234	.2256	21.20	.7100	.4485	28.23	.8576	.3757	19.48	.6964	.5077	20.64	.6976	.5097	23.53	.7770	.4134
MPR	26.08	.9025	.2505	21.07	.6985	.4503	27.09	.8318	.3692	19.42	.7046	.4983	20.31	.6907	.5172	22.80	.7656	.4171
NeRF+MPR	26.78	.9094	.2642	21.14	.7023	.4660	27.33	.8388	.4063	19.79	.7131	.5161	20.56	.6936	.5504	23.12	.7714	.4406
SRN	28.11	.9216	.1943	22.96	.7752	.3384	28.58	.8705	.2882	19.80	.7202	.4208	21.30	.7297	.4160	24.15	.8034	.3315
NeRF+SRN	28.29	.9271	.2073	23.22	.7900	.3309	28.88	.8812	.2964	20.11	.7340	.4238	21.61	.7448	.4215	24.42	.8154	.3360
Deblur-NeRF	28.49	.9275	.1993	21.67	.7213	.4431	27.99	.8581	.3527	18.99	.6685	.4843	20.65	.6915	.4914	23.56	.7734	.3942
BAD-NeRF	28.80	.9278	.1872	20.39	.6696	.4052	29.46	.8867	.2416	20.35	.7475	.3363	22.10	.7540	.3831	24.22	.7971	.3107
E ² NeRF	30.17	.9459	.1057	27.90	.9046	.2638	29.29	.8841	.2420	24.02	.8625	.2906	25.63	.8688	.2919	27.40	.8932	.2388
EBAD-NeRF	30.53	.9475	.1120	28.10	.9085	0.159	31.50	.9193	.1607	24.91	.8783	.2071	26.66	.8732	.2230	28.30	.9031	.1749

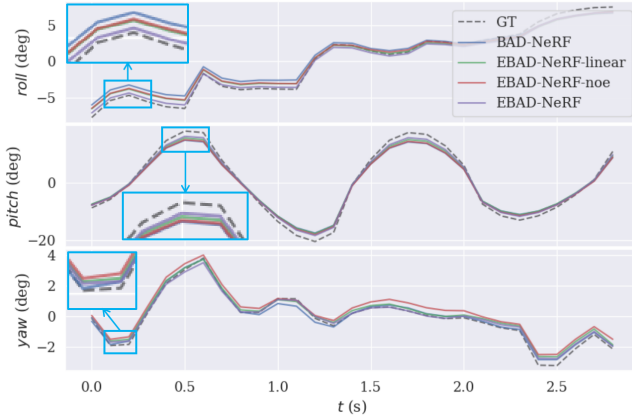


Figure 4: Ablation study of trajectory fitting accuracy on Tanabata scene. EBAD-NeRF-linear and EBAD-NeRF-noe are defined in Sec. 4.3. The figure shows that the event-driven bundle adjustment significantly fits the camera motion closer to the ground truth in the roll, pitch, and yaw metrics than other methods.

(BAD-NeRF) is even worse than the unconstrained bundle adjustment (EBAD-NeRF-noe) for fitting irregular camera motions. The same conclusion will be obtained by comparing EBAD-NeRF-linear and EBAD-NeRF-full, both with event enhancement.

4.3.2 Effect of Linear Event in Bundle Adjustment: Comparing BAD-NeRF and EBAD-NeRF-linear, even with the negative impact of linear interpolation bundle adjustment in Table 2, EBAD-NeRF-linear still has improvements in trajectory fitting and reconstruction results. Comparing EBAD-NeRF-linear and EBAD-NeRF under the constraints of event information, event-driven bundle adjustment achieved the best trajectory fitting and reconstruction results.

To sum up, during the NeRF training, event data can not only provide image-level optimization information but also pose-level practical constraints. Our proposed EBAD-NeRF effectively utilizes the ERGB-dual-modal data to achieve this goal. The qualitative comparison in Figure 3 and Figure 4 also testify to this.

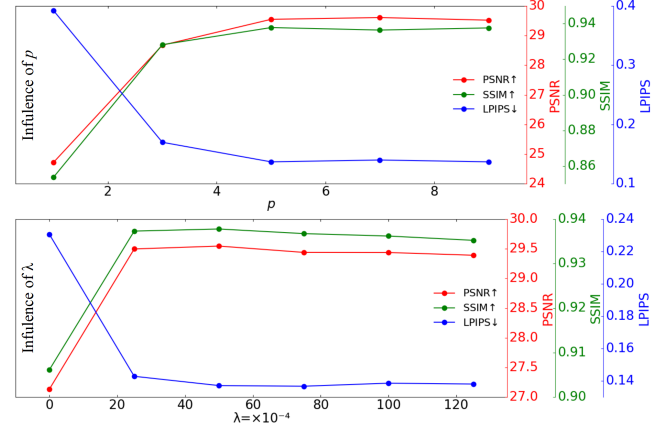


Figure 5: The influence of the number of learnable poses p and the weight parameter λ on the Cozyroom scene. The results are average for reconstructed images from both deblurring and novel views.

4.4 Analysis on Parameters

We evaluate the rendering results on the Cozyroom scene to analyze the superparameters p and λ of the proposed network. The red, green, and blue lines in Figure 5 represent PSNR, SSIM, and LPIPS, respectively.

4.4.1 The influence of b : Intuitively, the more virtual sharp frames, the more accurate the simulation of camera motion blur, and the corresponding network learning results will be better. The results in Figure 5 are consistent with this. When the number of virtual frames gradually increases from 1, the performance of the network also becomes significantly better. After exceeding 5, the number of virtual frames has almost no impact on the reconstruction results. Therefore, $p = 5$ is set in our experiments.

4.4.2 The influence of λ : As shown in Figure 5, λ has the best effect when set to 0.005, and if the weight of event loss is further increased, the network performance will gradually decrease.

Table 4: Quantitative Results on Novel Views of Blender Scenes. The Best Results are Shown in Bold

	Cozyroom			Factory			Pool			Tanabata			Wine			Average		
	PSNR↑	SSIM↑	LPIPS↓															
NeRF	26.98	.9021	.2875	20.58	.6953	.5226	27.22	.8345	.4320	19.12	.6882	.5654	19.91	.6763	.5852	22.76	.7593	.4785
NeRF+D2Net	28.02	.9219	.2264	21.49	.7345	.4490	28.04	.8582	.3745	19.70	.7181	.4990	20.43	.7137	.5092	23.54	.7893	.4116
NeRF+MPR	26.60	.9066	.2665	22.08	.7355	.4629	27.20	.8368	.4045	19.81	.7183	.5112	20.45	.6968	.5513	23.23	.7788	.4393
NeRF+SRN	28.21	.9251	.2076	23.18	.8018	.3300	28.78	.8808	.2939	21.03	.7708	.4133	21.99	.7637	.4203	24.64	.8284	.3330
Deblur-NeRF	28.42	.9260	.2000	22.12	.7490	.4369	27.92	.8594	.3491	20.77	.7412	.4605	21.13	.7128	.4859	24.07	.7977	.3865
BAD-NeRF	28.52	.9250	.1918	21.11	.7169	.4077	29.70	.8919	.2376	22.37	.8102	.3267	22.79	.7791	.3812	24.90	.8246	.3090
E ² NeRF	30.07	.9469	.1062	27.78	.9090	.2654	29.34	.8905	.2374	24.25	.8730	.2882	25.70	.8772	.2910	27.43	.8993	.2376
EBAD-NeRF	30.60	.9476	.1138	28.25	.9146	.1583	31.62	.9244	.1559	25.45	.8898	.2056	26.72	.8889	.1961	27.80	.9131	.1784

Table 5: Quantitative Results on Real Scenes. The Results are the Average of the Scenes, and The Best Results are Shown in Bold.

	NeRF	NeRF+D2Net	NeRF+MPR	NeRF+SRN	Deblur-NeRF	BAD-NeRF	E ² NeRF	EBAD-NeRF
PSNR↑	24.87	26.31	24.35	25.91	25.59	28.10	27.78	29.60
SSIM↑	.8562	.8829	.8539	.8706	.8744	.8839	.9062	.9175
LPIPS↓	.5005	.4092	.4963	.4198	.3885	.3632	.2403	.2156

Table 6: Absolute Trajectory Error Results of Blender Scenes.

	ATE
COLMAP-Blur (NeRF [29])	0.0476 ± 0.0171
COLMAP-EDI (E ² NeRF [33])	0.0419 ± 0.0159
Linear Bundle Adjustment (BAD-NeRF [44])	0.0462 ± 0.0142
Event-driven Bundle Adjustment (Ours)	0.0383 ± 0.0143

4.5 Quantitative Results

4.5.1 Quantitative Results of Reconstruction on Blender Scenes: In Tables 3 and 4, we evaluate the reconstruction results of learned neural radiance fields in five blender scenarios from deblurring and novel views, respectively. SRN and SRN+NeRF achieve the best results in single-image-based deblurring methods. With the help of event data, D2Net is also slightly better than MPR. For Deblur-NeRF and BAD-NeRF, although they have been further improved compared to NeRF+D2Net, NeRF+MPR, and NeRF+SRN, they still cannot surpass event-enhanced E²NeRF and our proposed EBAD-NeRF. Note that there is no apparent difference between the E²NeRF and EBAD-NeRF on the Cozyroom scene where linear camera shake produces motion blur, and E²NeRF is even better than EBAD-NeRF on LPIPS. However, in the other four scenes with more complex camera shaking as described in Sec. 4.1, the results of EBAD-NeRF in both deblurring views and novel views are significantly better than E²NeRF, which indicates that lacking the optimization of poses limits the role of events in 3D reconstruction in E²NeRF, especially when facing complex camera motion. Accordingly, EBAD-NeRF uses event-driven bundle adjustment to jointly optimize the motion poses of the camera, further releasing the potential of event data in reconstructing a sharp NeRF with blurry images.

4.5.2 Quantitative Results of Pose Estimation on Blender Scenes: In Table 6, we use absolute trajectory error to evaluate the accuracy

of camera motion trajectory estimation by different methods. The results in the table are the average of five blender scenes. COLMAP-Blur means directly inputting the blurry images into COLMAP to estimate the camera poses of each view. This is a typical pose estimation method in NeRF-related work. COLMAP-EDI represents the method used in E²NeRF. It uses the EDI [32] algorithm to first use events to deblur the image and then input the sharp image sequence into COLMAP to estimate camera poses of the blur process. Linear bundle adjustment represents the linear interpolation method used by BAD-NeRF to jointly learn the pose changes of each view. Our proposed event-driven bundle adjustment method introduces event into joint learning of camera pose changes and sharp NeRF, achieving the best results in restoring the camera pose, which also promotes EBAD-NeRF to further improve the reconstruction quantification results as in Tables 3 and 4.

4.5.3 Quantitative Reconstruction Results on Blender Scenes: To verify the effectiveness of our method on real data, we conducted experiments with two real scenes captured by DAVIS-346. As shown in Table 5, the comparison results with other methods are highly consistent with the results on blender scenes in Tables 3 and 4, which verifies the reliability of our method in practical applications.

4.6 Qualitative Results

4.6.1 Qualitative Results of Reconstruction on Blender Scenes. As shown in Figure 6 and the first and second row in Figure 7, we compared the results of the synthesis deblurring view on the pool scene and novel view on the Wine and Factory scenes, respectively. For the deblurring view results, the results of EBAD-NeRF are sharper than other state-of-the-art single-image deblurring methods, event-RGB-based deblurring methods, and deblurring NeRF methods. For the green plants and wooden boxes in the scene, some artifacts appear in the results of E²NeRF, and our method effectively recovers the texture details. In the Wine and Factory scenes, though E²NeRF

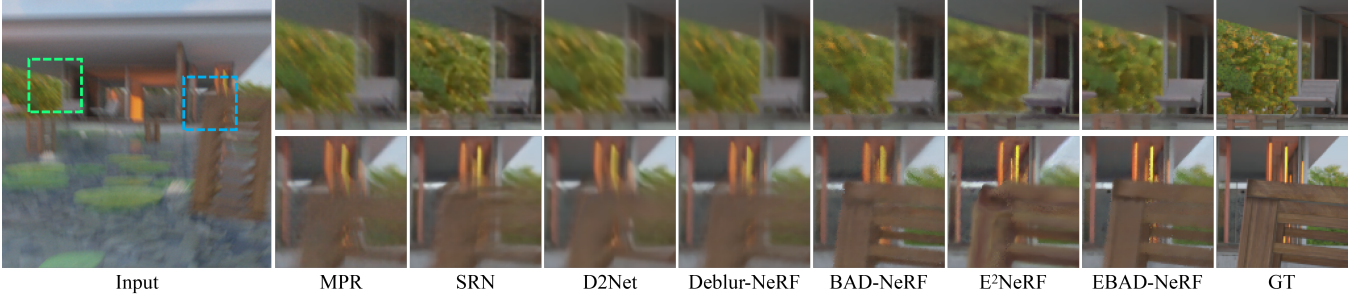


Figure 6: Qualitative results of deblurring views on blender Pool scene.

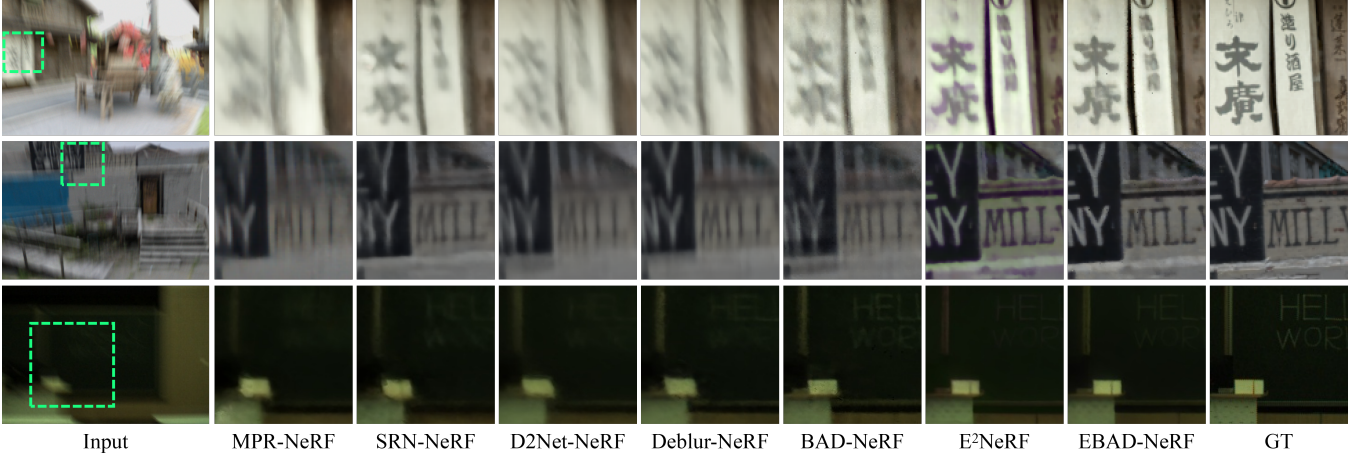


Figure 7: Qualitative results of novel views on blender Wine and Factory scenes (first and second row), real scene (third row).

realizes noticeable results for the characters and letters, our method is closer to ground truth in color, clarity, and line thickness.

4.6.2 Qualitative Results of Pose Estimation on Blender Scenes. In Figure 8, we compare the estimated camera trajectory of different methods from the three dimensions of roll, pitch, and yaw. The purple curve representing EBAD-NeRF is the closest to the dashed line representing ground truth, which is consistent with the quantitative data in Table 6.

4.6.3 Qualitative Results on Real Scenes. As in the third row of Figure 7, our method better recovers the white letters on the blackboard, compared to the pose-fixed event-RGB-based method E²NeRF, while BAD-NeRF is limited in reconstructing smooth areas (white areas on the podium). The results of other image-deblurring-NeRF methods and Deblur-NeRF are all limited by the severe blurry input, which is the same as the quantitative results in Table 5.

Experiments on synthetic and real data show that our method can learn better poses of the camera motion blur process with event-driven bundle adjustment compared to the previous deblurring NeRF method. On this basis, the event data is also superimposed on the image blur process supervision, eventually achieving better 3D reconstruction and novel view synthesis effects.

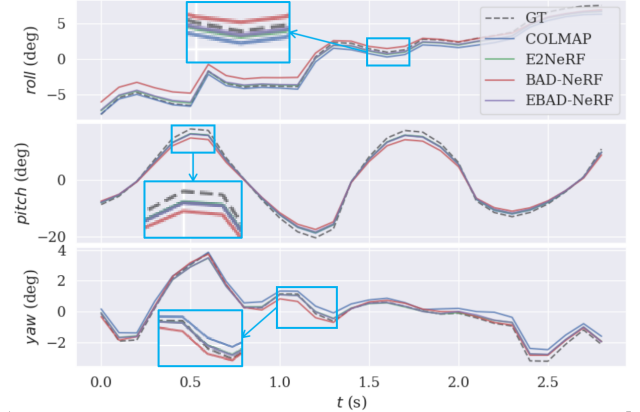


Figure 8: Qualitative evaluation of trajectory fitting accuracy on Tanabata scene. The figure shows that the event-driven bundle adjustment significantly fits the camera motion closer to the ground truth in the roll, pitch, and yaw metrics than other methods. Note that though there is event enhancement on blurry image formation in E²NeRF, the motion trajectory is distorted and leads to the inaccurate NeRF.

5 CONCLUSION

In conclusion, this paper presents a novel approach, leveraging event-driven bundle adjustment, to address the challenge of modeling camera motion blur within neural radiance fields (NeRFs). Our framework draws inspiration from the emerging field of event-based vision, which offers high temporal resolution and asynchronous events, ideal for capturing dynamic scenes with motion blur. By integrating intensity-change-metric event loss and photo-metric blur loss, our framework enables the simultaneous optimization of blur modeling alongside NeRF reconstruction. Experiments on synthetic and real-world datasets demonstrate the efficacy of our approach in accurately estimating camera poses and producing sharp NeRF reconstructions.

REFERENCES

- [1] Himanshu Akolkar, Sio-Hoi Ieng, and Ryad Benosman. 2020. Real-time high speed motion prediction using fast aperture-robust event-driven visual flow. *IEEE Transactions on Pattern Analysis and Machine Intelligence* 44, 1 (2020), 361–372.
- [2] Jonathan T Barron, Ben Mildenhall, Matthew Tancik, Peter Hedman, Ricardo Martin-Brualla, and Pratul P Srinivasan. 2021. Mip-nerf: A multiscale representation for anti-aliasing neural radiance fields. In *Proceedings of the IEEE/CVF International Conference on Computer Vision*. 5855–5864.
- [3] Jonathan T Barron, Ben Mildenhall, Dor Verbin, Pratul P Srinivasan, and Peter Hedman. 2022. Mip-nerf 360: Unbounded anti-aliased neural radiance fields. In *Proceedings of the IEEE/CVF Conference on Computer Vision and Pattern Recognition*. 5470–5479.
- [4] Calin Belha and Vijay Kumar. 2002. Euclidean metrics for motion generation on SE (3). *Proceedings of the Institution of Mechanical Engineers, Part C: Journal of Mechanical Engineering Science* 216, 1 (2002), 47–60.
- [5] Wenjing Bian, Zirui Wang, Kejie Li, and Jia-Wang Bian. 2023. NoPe-NeRF: Optimising Neural Radiance Field with No Pose Prior. In *2023 IEEE/CVF Conference on Computer Vision and Pattern Recognition (CVPR)*. 4160–4169. <https://doi.org/10.1109/CVPR52729.2023.00405>
- [6] Tony F Chan and Chiu-Kwong Wong. 1998. Total variation blind deconvolution. *IEEE transactions on Image Processing* 7, 3 (1998), 370–375.
- [7] Zhiqin Chen, Thomas Funkhouser, Peter Hedman, and Andrea Tagliasacchi. 2023. Mobilernerf: Exploiting the polygon rasterization pipeline for efficient neural field rendering on mobile architectures. In *Proceedings of the IEEE/CVF Conference on Computer Vision and Pattern Recognition*. 16569–16578.
- [8] Guillermo Gallego, Tobi Delbrück, Garrick Orchard, Chiara Bartolozzi, Brian Taba, Andrea Censi, Stefan Leutenegger, Andrew J Davison, Jörg Conradt, Kostas Daniilidis, et al. 2020. Event-based vision: A survey. *IEEE transactions on pattern analysis and machine intelligence* 44, 1 (2020), 154–180.
- [9] Kyle Gao, Yina Gao, Hongjie He, Denling Lu, Linlin Xu, and Jonathan Li. 2022. Nerf: Neural radiance field in 3d vision, a comprehensive review. *arXiv preprint arXiv:2210.00379* (2022).
- [10] Stephan J Garbin, Marek Kowalski, Matthew Johnson, Jamie Shotton, and Julien Valentin. 2021. Fastrnerf: High-fidelity neural rendering at 200fps. In *Proceedings of the IEEE/CVF International Conference on Computer Vision*. 14346–14355.
- [11] Mathias Gehrig, Mario Millhäuser, Daniel Gehrig, and Davide Scaramuzza. 2021. E-raft: Dense optical flow from event cameras. In *2021 International Conference on 3D Vision (3DV)*. IEEE, 197–206.
- [12] Michael Grupp. 2017. evo: Python package for the evaluation of odometry and SLAM. <https://github.com/MichaelGrupp/evo>.
- [13] Jesse Hagenauer, Federico Paredes-Vallés, and Guido De Croon. 2021. Self-supervised learning of event-based optical flow with spiking neural networks. *Advances in Neural Information Processing Systems* 34 (2021), 7167–7179.
- [14] Kaiming He, Xiangyu Zhang, Shaoqing Ren, and Jian Sun. 2016. Deep residual learning for image recognition. In *Proceedings of the IEEE conference on computer vision and pattern recognition*. 770–778.
- [15] Tao Hu, Shu Liu, Yilun Chen, Tiancheng Shen, and Jiaya Jia. 2022. Efficientnerf: efficient neural radiance fields. In *Proceedings of the IEEE/CVF Conference on Computer Vision and Pattern Recognition*. 12902–12911.
- [16] Yuhuang Hu, Shih-Chii Liu, and Tobi Delbrück. 2021. v2e: From video frames to realistic DVS events. In *Proceedings of the IEEE/CVF Conference on Computer Vision and Pattern Recognition*. 1312–1321.
- [17] Inwoo Hwang, Junho Kim, and Young Min Kim. 2023. Ev-NeRF: Event based neural radiance field. In *Proceedings of the IEEE/CVF Winter Conference on Applications of Computer Vision*. 837–847.
- [18] Zhe Jiang, Yu Zhang, Dongqing Zou, Jimmy Ren, Jiancheng Lv, and Yebin Liu. 2020. Learning event-based motion deblurring. In *Proceedings of the IEEE/CVF Conference on Computer Vision and Pattern Recognition*. 3320–3329.
- [19] Tae Hyun Kim, Seungjun Nah, and Kyoung Mu Lee. 2016. Dynamic scene deblurring using a locally adaptive linear blur model. *arXiv preprint arXiv:1603.04265* (2016).
- [20] Dilip Krishnan, Terence Tay, and Rob Fergus. 2011. Blind deconvolution using a normalized sparsity measure. In *CVPR 2011*. IEEE, 233–240.
- [21] Byeonghyeon Lee, Howoong Lee, Usman Ali, and Eunbyung Park. 2024. Sharp-NeRF: Grid-based Fast Deblurring Neural Radiance Fields Using Sharpness Prior. In *Proceedings of the IEEE/CVF Winter Conference on Applications of Computer Vision*. 3709–3718.
- [22] Dogyoon Lee, Minhyeok Lee, Chajin Shin, and Sangyoun Lee. 2023. Dp-nerf: Deblurred neural radiance field with physical scene priors. In *Proceedings of the IEEE/CVF Conference on Computer Vision and Pattern Recognition*. 12386–12396.
- [23] Chen-Hsuan Lin, Wei-Chin Ma, Antonio Torralba, and Simon Lucey. 2021. BARF: Bundle-Adjusting Neural Radiance Fields. In *2021 IEEE/CVF International Conference on Computer Vision (ICCV)*. 5721–5731. <https://doi.org/10.1109/ICCV48922.2021.00569>
- [24] Songnan Lin, Jiawei Zhang, Jinshan Pan, Zhe Jiang, Dongqing Zou, Yongtian Wang, Jing Chen, and Jimmy Ren. 2020. Learning event-driven video deblurring and interpolation. In *European Conference on Computer Vision*. Springer, 695–710.
- [25] Weng Fei Low and Gim Hee Lee. 2023. Robust e-NeRF: NeRF from Sparse & Noisy Events under Non-Uniform Motion. In *Proceedings of the IEEE/CVF International Conference on Computer Vision*. 18335–18346.
- [26] Li Ma, Xiaoyu Li, Jing Liao, Qi Zhang, Xuan Wang, Jue Wang, and Pedro V Sander. 2022. Deblur-NeRF: Neural Radiance Fields from Blurry Images. In *Proceedings of the IEEE/CVF Conference on Computer Vision and Pattern Recognition*. 12861–12870.
- [27] Qi Ma, Danda Pani Paudel, Ajad Chhatkuli, and Luc Van Gool. 2023. Deformable Neural Radiance Fields using RGB and Event Cameras. In *Proceedings of the IEEE/CVF International Conference on Computer Vision*. 3590–3600.
- [28] Ben Mildenhall, Peter Hedman, Ricardo Martin-Brualla, Pratul P Srinivasan, and Jonathan T Barron. 2022. Nerf in the dark: High dynamic range view synthesis from noisy raw images. In *Proceedings of the IEEE/CVF Conference on Computer Vision and Pattern Recognition*. 16190–16199.
- [29] Ben Mildenhall, Pratul P Srinivasan, Matthew Tancik, Jonathan T Barron, Ravi Ramamoorthi, and Ren Ng. 2021. Nerf: Representing scenes as neural radiance fields for view synthesis. *Commun. ACM* 65, 1 (2021), 99–106.
- [30] Michael Niemeyer, Jonathan T Barron, Ben Mildenhall, Mehdi SM Sajjadi, Andreas Geiger, and Noha Radwan. 2022. Regnerf: Regularizing neural radiance fields for view synthesis from sparse inputs. In *Proceedings of the IEEE/CVF Conference on Computer Vision and Pattern Recognition*. 5480–5490.
- [31] Liyuan Pan, Miaomiao Liu, and Richard Hartley. 2020. Single image optical flow estimation with an event camera. In *2020 IEEE/CVF Conference on Computer Vision and Pattern Recognition (CVPR)*. IEEE, 1669–1678.
- [32] Liyuan Pan, Cedric Scheerlinck, Xin Yu, Richard Hartley, Miaomiao Liu, and Yuchao Dai. 2019. Bringing a blurry frame alive at high frame-rate with an event camera. In *Proceedings of the IEEE/CVF Conference on Computer Vision and Pattern Recognition*. 6820–6829.
- [33] Yunshan Qi, Lin Zhu, Yu Zhang, and Jia Li. 2023. E2NeRF: Event Enhanced Neural Radiance Fields from Blurry Images. In *Proceedings of the IEEE/CVF International Conference on Computer Vision*. 13254–13264.
- [34] Viktor Rudnev, Mohamed Elgharib, Christian Theobalt, and Vladislav Golyanik. 2023. EventNeRF: Neural radiance fields from a single colour event camera. In *Proceedings of the IEEE/CVF Conference on Computer Vision and Pattern Recognition*. 4992–5002.
- [35] Wei Shang, Dongwei Ren, Dongqing Zou, Jimmy S Ren, Ping Luo, and Wangmeng Zuo. 2021. Bringing events into video deblurring with non-consecutively blurry frames. In *Proceedings of the IEEE/CVF International Conference on Computer Vision*. 4531–4540.
- [36] Shintaro Shiba, Yoshimitsu Aoki, and Guillermo Gallego. 2022. Secrets of event-based optical flow. In *European Conference on Computer Vision*. Springer, 628–645.
- [37] Hyeongseok Son, Junyong Lee, Jonghyeop Lee, Sunghyun Cho, and Seungyong Lee. 2021. Recurrent video deblurring with blur-invariant motion estimation and pixel volumes. *ACM Transactions on Graphics (TOG)* 40, 5 (2021), 1–18.
- [38] Shuochen Su, Mauricio Delbracio, Jue Wang, Guillermo Sapiro, Wolfgang Heidrich, and Oliver Wang. 2017. Deep video deblurring for hand-held cameras. In *Proceedings of the IEEE conference on computer vision and pattern recognition*. 1279–1288.
- [39] Lei Sun, Christos Sakaridis, Jingyun Liang, Qi Jiang, Kailun Yang, Peng Sun, Yaozu Ye, Kaiwei Wang, and Luc Van Gool. 2022. Event-based fusion for motion deblurring with cross-modal attention. In *European conference on computer vision*. Springer, 412–428.
- [40] Xin Tao, Hongyun Gao, Xiaoyong Shen, Jue Wang, and Jiaya Jia. 2018. Scale-recurrent network for deep image deblurring. In *Proceedings of the IEEE conference on computer vision and pattern recognition*. 8174–8182.
- [41] Xin Tao, Hongyun Gao, Xiaoyong Shen, Jue Wang, and Jiaya Jia. 2018. Scale-Recurrent Network for Deep Image Deblurring. In *2018 IEEE/CVF Conference on Computer Vision and Pattern Recognition*. 8174–8182.

- [42] Gemma Taverni, Diederik Paul Moeyns, Chenghan Li, Celso Cavaco, Vasyl Motsnyi, David San Segundo Bello, and Tobi Delbrück. 2018. Front and back illuminated dynamic and active pixel vision sensors comparison. *IEEE Transactions on Circuits and Systems II: Express Briefs* 65, 5 (2018), 677–681.
- [43] Dor Verbin, Peter Hedman, Ben Mildenhall, Todd Zickler, Jonathan T Barron, and Pratul P Srinivasan. 2022. Ref-nerf: Structured view-dependent appearance for neural radiance fields. In *2022 IEEE/CVF Conference on Computer Vision and Pattern Recognition (CVPR)*. IEEE, 5481–5490.
- [44] Peng Wang, Lingzhe Zhao, Ruiji Ma, and Peidong Liu. 2023. BAD-NeRF: Bundle Adjusted Deblur Neural Radiance Fields. In *Proceedings of the IEEE/CVF Conference on Computer Vision and Pattern Recognition*. 4170–4179.
- [45] Patrick Wieschollek, Michael Hirsch, Bernhard Schölkopf, and Hendrik Lensch. 2017. Learning blind motion deblurring. In *Proceedings of the IEEE international conference on computer vision*. 231–240.
- [46] Patrick Wieschollek, Bernhard Schölkopf, Hendrik Lensch, and Michael Hirsch. 2016. End-to-end learning for image burst deblurring. In *asian conference on computer vision*. Springer, 35–51.
- [47] Fang Xu, Lei Yu, Bishan Wang, Wen Yang, Gui-Song Xia, Xu Jia, Zhendong Qiao, and Jianzhuang Liu. 2021. Motion deblurring with real events. In *Proceedings of the IEEE/CVF International Conference on Computer Vision*. 2583–2592.
- [48] Lan Xu, Weipeng Xu, Vladislav Golyanik, Marc Habermann, Lu Fang, and Christian Theobalt. 2020. Eventcap: Monocular 3d capture of high-speed human motions using an event camera. In *Proceedings of the IEEE/CVF Conference on Computer Vision and Pattern Recognition*. 4968–4978.
- [49] Li Xu, Shicheng Zheng, and Jiaya Jia. 2013. Unnatural l0 sparse representation for natural image deblurring. In *Proceedings of the IEEE conference on computer vision and pattern recognition*. 1107–1114.
- [50] Qiangeng Xu, Zexiang Xu, Julien Philip, Sai Bi, Zhixin Shu, Kalyan Sunkavalli, and Ulrich Neumann. 2022. Point-nerf: Point-based neural radiance fields. In *Proceedings of the IEEE/CVF conference on computer vision and pattern recognition*. 5438–5448.
- [51] Mingyuan Yao, Yukang Huo, Yang Ran, Qingbin Tian, Rui Feng Wang, and Haihua Wang. 2024. Neural Radiance Field-based Visual Rendering: A Comprehensive Review. *arXiv preprint arXiv:2404.00714* (2024).
- [52] Alex Yu, Vickie Ye, Matthew Tancik, and Angjoo Kanazawa. 2021. pixelnerf: Neural radiance fields from one or few images. In *Proceedings of the IEEE/CVF Conference on Computer Vision and Pattern Recognition*. 4578–4587.
- [53] Syed Waqas Zamir, Aditya Arora, Salman Khan, Munawar Hayat, Fahad Shahbaz Khan, Ming-Hsuan Yang, and Ling Shao. 2021. Multi-stage progressive image restoration. In *Proceedings of the IEEE/CVF conference on computer vision and pattern recognition*. 14821–14831.
- [54] Syed Waqas Zamir, Aditya Arora, Salman Khan, Fahad Shahbaz Khan, and Ling Shao. 2021. Learning digital camera pipeline for extreme low-light imaging. *Neurocomputing* 452 (2021), 37–47.
- [55] Haichao Zhang and Lawrence Carin. 2014. Multi-shot imaging: joint alignment, deblurring and resolution-enhancement. In *Proceedings of the IEEE Conference on Computer Vision and Pattern Recognition*. 2925–2932.
- [56] Haichao Zhang and Jianchao Yang. 2015. Intra-frame deblurring by leveraging inter-frame camera motion. In *Proceedings of the IEEE Conference on Computer Vision and Pattern Recognition*. 4036–4044.
- [57] Jiqing Zhang, Bo Dong, Haiwei Zhang, Jianchuan Ding, Felix Heide, Baocai Yin, and Xin Yang. 2022. Spiking Transformers for Event-Based Single Object Tracking. In *Proceedings of the IEEE/CVF Conference on Computer Vision and Pattern Recognition*. 8801–8810.
- [58] Jiqing Zhang, Xin Yang, Yingkai Fu, Xiaopeng Wei, Baocai Yin, and Bo Dong. 2021. Object tracking by jointly exploiting frame and event domain. In *Proceedings of the IEEE/CVF International Conference on Computer Vision*. 13043–13052.
- [59] Kaihao Zhang, Wenhan Luo, Yiran Zhong, Lin Ma, Bjorn Stenger, Wei Liu, and Hongdong Li. 2020. Deblurring by realistic blurring. In *Proceedings of the IEEE/CVF Conference on Computer Vision and Pattern Recognition*. 2737–2746.
- [60] Richard Zhang, Phillip Isola, Alexei A Efros, Eli Shechtman, and Oliver Wang. 2018. The unreasonable effectiveness of deep features as a perceptual metric. In *Proceedings of the IEEE conference on computer vision and pattern recognition*. 586–595.